

## Drop Formation At A T-Junction With Dilute Xanthan Gum Solutions As The Dispersed Phase

J. L. Liow<sup>1</sup> and Z. P. Gu<sup>1</sup>

<sup>1</sup>School of Engineering and Information Technology  
The University of New South Wales ADFA. Canberra, ACT 2600

### Abstract

Drops were formed at a T-junction with dilute xanthan gum (XG) solutions of 0.01, 0.025 and 0.05 wt% as the dispersed phase fluid. The continuous phase was a Newtonian fluid, canola oil, with a viscosity of 0.065 Pa.s. The drop diameter was found to decrease with increasing continuous phase flow rate. A more structured approach for delineating the different drop formation employing the change in drop diameter with the continuous phase Capillary number ( $Ca_c$ ) was found to work well with the data obtained as well as with published data. The results showed that a higher viscosity for the dispersed phase fluid results in a smaller value of  $Ca_c$  for the transition from the dripping to jetting drop formation regime but did not have a strong influence on the transition from the squeezing to dripping drop formation regime.

### Introduction

The production of drops in microfluidic devices have been used to control chemical reactions, enable protein crystallisation, perform DNA and blood analysis, process food, enhance material production, fast-track drug discovery, perform fluidic logic functions and enhance health-care products. The drops formed can be controlled to produce a narrow size distribution with less than 5% variation; unlike the traditional top-down methods of emulsion and particle formation.

The droplet formation process can be categorized into different regimes, namely the squeezing ( $Ca_c < 0.01$ ), dripping ( $0.02 < Ca_c < 0.2$ ) and jetting ( $Ca_c > 0.3$ ) regimes, where the continuous phase Capillary number is used ( $Ca_c = u_c \mu_c / \sigma$ , where  $u_c$  and  $\mu_c$  are the velocity and viscosity of the continuous phase respectively, and  $\sigma$  is the interfacial tension). Current methods for identification of the different regimes require adequate and quantitative descriptions of each regime and its corresponding mechanism. Hitherto, the methods commonly used to identify various droplet formation regimes include:

- Using droplet formation pictures, in which large droplets confined by the main channel are classified as in the squeezing regime, medium-sized droplets that partly fill the main channel being the dripping regime, and small droplets accompanied by a long filament as the jetting regime [10, 12]. This method provides a clear visual impression of how droplets are produced in each regime but involves significant effort and can be subjective.
- Plotting the length of the droplet (or equivalent spherical diameter) against  $Ca_c$  on log-log or semi-log coordinates through which the transition point can be identified by changes in the power law dependence of the droplet diameter for the variable studied [5, 10]. However, the transitional  $Ca_c$ , which is influenced by the viscosity ratio ( $\lambda = \mu_d / \mu_c$ ), may not be easily discerned. Others [2, 4] have shown that a higher viscosity ratio results in a clear transitional  $Ca_c$ , it is difficult to identify such a transitional  $Ca_c$  from the results [3] when a small viscosity ratio ( $\lambda < 0.01$ ) is employed.

- Using a phase diagram to distinguish between different droplet formation regimes [1]. This method not only requires extensive amount of data for the construction of the diagram but are limited to only a two or three variables.
- Using boundary conditions [11]. As droplets in contact channel walls with different properties, they are subject to different boundary conditions and this can be used to identify the droplet formation regimes. The transition from the dripping to jetting regimes is claimed to happen when the droplet diameter equals the depth of the main channel.

None of the above methods is of sufficient generality to identify the various formation regimes and provide a definitive  $Ca_c$  to separate the droplet formation regimes and there is no preferred method over another. As such, there is an urgent need for a more general method for identifying different droplet formation regimes and the transitional Capillary numbers.

There has been limited studies on the influence of non-Newtonian fluids on the different drop formation regimes. Hunsy and Cooper-white [8] showed that with either Newtonian fluids or non-Newtonian elastic fluids as the dispersed phase, the droplet size increased with decreasing  $\mu_c$  and is almost independent of  $\mu_d$ . Modelling work by Sang *et al.* [?] for a power law continuous phase fluid suggested that the drop diameter decreases with increasing in the viscosity of the continuous phase but the odd kink in their geometry a short distance downstream from the T-junction had a severe influence on their results thus limiting any useful comparison with other published data.

In summary, the data available at present suggest that in the squeezing and dripping regimes, the droplet size is affected by the viscosity ratio but there is a lack of data on the effect of varying the dispersed phase viscosity and this can be important with biological fluids where the fluid viscosities are shear dependent. In this study, the effect of the continuous and dispersed phase viscosities on the droplet diameter was investigated. Xanthan gum (XG) solutions of various concentrations were used to see the effect of increasing viscosity with a shear thinning fluid on the droplet formation process. As a large fraction of biological fluids have a shear thinning behaviour, an understanding of the droplet formation at a T-junction with such fluids can aid in the development of microfluidic devices involving the flow of biological fluids in the microchannels.

### Experimental setup

#### T-junction

The T-junction microfluidic device used in this study (fig. 1) was fabricated on a 50.0 (L) × 30.0 (W) × 3.0 (H) mm poly (methyl methacrylate) (PMMA) wafer by micro-end-milling [9] and sealed with a PMMA cover plate by solvent bonding with acetone at room temperature. The average surface roughness ( $R_a$ ) of the micro end-milled channels varies from 50 – 100 nm. Holes were drilled through the PMMA cover plate for placement of short metal tubes which linked the channels to silicone

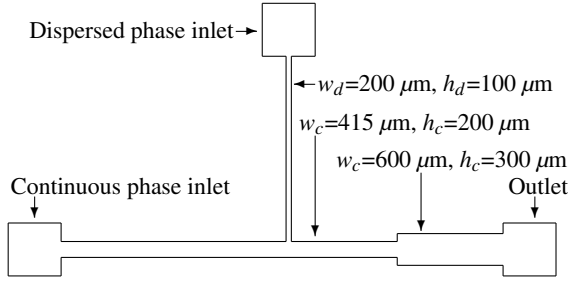


Figure 1: Schematic of the T-junction.

tubing. The silicon tubes were connected to two syringe pumps (Cole-Parmer 7600) that were used to independently control the flow rates of the continuous and dispersed phases into the microfluidic device. The main channel had an expansion zone located 2 mm after the T-junction which allowed the drop to acquire a spherical shape enabling its volume to be measured precisely.

### Materials

Canola oil was used as the continuous phase. Deionised water and different concentrations of XG (Sigma-Aldrich) solutions formulated with deionised water were used as the dispersed phase, all of which contained 0.5 wt% Tween 80 (Sigma-Aldrich). The viscosity was measured with a Brookfields DV-II+ viscometer, the interfacial tension with a KSV CAM 200 pendant-drop tensiometer, and the density with a density bottle; all at 20°C. The physical properties of the canola oil used for the continuous phase are a viscosity of 65.0 cp and density of 0.9149 g/ml and the interfacial tension with the dispersed phase are given in table 1 with the rest of the physical properties for the dispersed phase.

### Experimental

For each run, the continuous and dispersed flow rates were set from the syringe pump control pad. The flow was allowed to equilibrate for up to half an hour prior to taking measurements. The drop formation was observed through a Nikon SMZ1000 stereo-microscope and simultaneously filmed with a Redlake Motion Pro SI-4 high speed CCD video camera at 3000 fps. The outline of the drops were extracted using Mathematica and the pixels of the outline were saved for calculation of the drop volume. At least 50 drop were used to provide an average drop diameter and the drop size dispersity. The drop size was obtained by integrating slices along the axial direction of the profile assuming that each segment is circular if it was smaller than the channel depth and either a spheroidal or flattened disk if the segment was larger than the channel depth. The volume of the drop assuming either a spheroidal or flattened disk was found not differ greatly. The flattened disk results were used since the interfacial was quite low which meant the drops would deform easily at the wall boundaries. The drop volumes were obtained in both the main channel near the T-junction and in the expansion zone where it was usually spherical in shape. Although a large expansion zone would have enabled all drops to attain a spherical shape, the expansion zone could not be made too deep as it was necessary to ensure all drops videoed to be in focus. The drop formation times were measured for 10 or more drops and averaged. The dispersed phase flow rates were calculated from the drop volume and frequency. The continuous phase flow rate was more controllable and was determined by

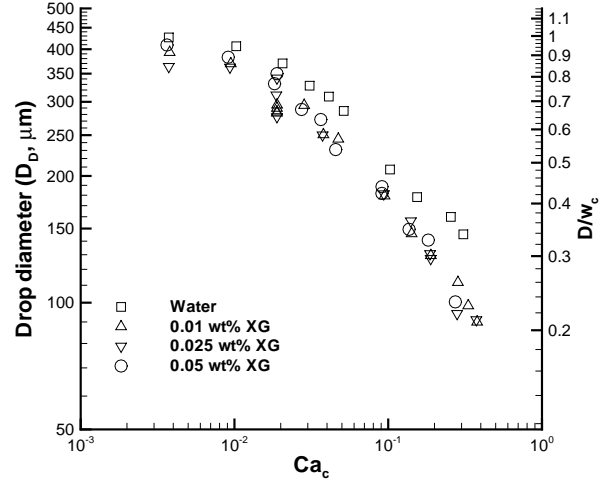


Figure 2: Drop diameter for varying  $Ca_c$  and wt % XG concentrations.  $Q_d = 0.1$  ml/hr.

calibrating the syringe pump prior to the experiment. The flow rates achievable was limited by the pressure drop, which in turn often led to much longer times for equilibration at high flow rates as the silicon tubing expanded slightly as the pressure drop required increased with increasing flow rates.

### Results

#### Drop Size for Varying Continuous Phase Flow Rate

Figure 2 shows the variation of the drop diameter with  $Ca_c$  for a fixed dispersed phase flow rate ( $Q_d$ ) of 0.1 ml/hr. The continuous phase flow rate was varied between 0.2 to 20.0 ml/hr ( $0.003 < Ca_c < 0.38$ ). At low  $Ca_c$  values ( $< 0.01$ ) where the drop diameter was comparable to the width of the main channel, the drop diameter decreased slowly with increasing  $Ca_c$  ( $\propto Q_c$ ). The drop size is expected to increase slowly with decreasing  $Ca_c$  since the drop length is proportional to  $Q_d/Q_c$  (i.e.,  $Ca_c^{-1}$ ) [3, 5] as the drop volume scales mainly to the dispersed phase flow rate. As  $Ca_c$  increases, the decrease in drop diameter suddenly increases and this is taken to signify the start of the dripping regime. The decrease in drop diameter is rapid at low  $Ca_c$  but slows down at higher  $Ca_c$  in agreement with previous investigators [8, 11]. De Menech [4] suggests a critical value of  $Ca_c = 0.015$  for transition from the squeezing to dripping mechanism, which is only weakly dependent on viscosity ratio, while other investigators [5, 3, 7, 6] have used a lower value of  $Ca_c = 0.01$ . On the log-log plot (figure 2) the change in drop diameter with  $Ca_c$  is smooth and no sharp changes in the gradient of the curves are noticeable, unlike De Menech simulations where a sharp transition to  $D_m \propto (Ca_c \dot{\epsilon}_d)^{-0.4}$  ( $\dot{\epsilon}_d = \epsilon w_c / \nu_c$  is the dimensionless shear rate) was found. The data for both the water and XG fit well with  $D_m \propto (Ca_c)^{-0.4}$  for  $0.02 < Ca_c < 0.2$ . Xu *et al.* [11] claimed that the scaling changes sharply from  $D_m \propto Ca_c^{-0.3}$  to  $D_m \propto Ca_c^{-1}$  at  $Ca_c = 0.1$  giving an abrupt changeover point for the dripping to jetting transition but our data does not support such an abrupt transition. The results of figure 2 suggests that there is a trend that the slope does increase for  $Ca_c > 0.2$  but there is insufficient data points over a suitable range available to provide a good fit to confirm the  $D_m \propto Ca_c^{-1}$  scaling occurs for  $Ca_c > 0.2$ .

There was no clear difference in the drop size for the different concentrations of XGs although the drop size for the deionised

Solution	Power law		Carreau model			Interfacial tension (mN/m)	Density (g/ml)
	$k$ (Pa·s)	$n$	$\mu_0$ (Pa·s)	$\lambda$ (s)	$n$		
Water	0.00104	1.000	—	—	—	10.5	0.998
0.01 wt% XG	0.00130	1.000	—	—	—	10.7	0.998
0.025 wt% XG	0.00202	1.000	—	—	—	11.5	0.998
0.05 wt% XG	0.0395	0.722	0.12	28.0	0.647	12.3	0.998

Table 1: Physical properties of the dispersed phase.

water case was generally larger than those of the XGs, the difference being more pronounced at higher values of  $Ca_c$ . Repeats for a few values showed that the smaller drop diameters for the XGs were reproducible. The lack of dependence on the XG viscosity is in agreement with the results of Husny and Cooper-White [8] where the drop formation process was found to be governed by the continuous phase properties. The non-Newtonian effects exhibit themselves mainly during the drop breakup stage where localised shear rates are large.

#### Delineation of the Different Drop Formation Regimes

Since the values of  $Ca_c$  that delineates the transition between the different droplet formation regimes is still rather subjective, we propose a new method for determining such transitional  $Ca_c$  by using the slope of  $dD_D/dCa_c$  obtained from fitting the droplet diameter ( $D_D$ ) as a function of  $Ca_c$ . Each set of results in figure 2 was fitted with a third-order polynomial and the slopes of  $dD_D/dCa_c$  were then plotted against  $Ca_c$  in figure 3. Figure 3 was compared with the images from the experiments and they showed that the dripping to jetting transition corresponded to the peak in the slope, while the squeezing to dripping transition corresponded to the region where the slope was starting to rise. The second order differential,  $d^2D_D/dCa_c^2$ , of the third order fit is shown in figure 4 for the 0.05 wt% xanthan gum solution. In the low  $Ca_c$  region,  $d^2D_D/dCa_c^2$  shows a small constant negative slope before a larger increase in the negative slope. The sudden change in the negative slope in the slope of  $d^2D_D/dCa_c^2$  in figure 4 corresponds to the squeezing to dripping transitional  $Ca_c$  and provides a much clearer criterion for identification. The peak in the slope can be identified by the zero crossing of  $d^2D_D/dCa_c^2$  in figure 4 and is identified with the transitional  $Ca_c$  for dripping to jetting.

This simple method of obtaining the transitional  $Ca_c$  is less subjective. We find that the squeezing to dripping regimes generally falls between  $0.01 < Ca_c < 0.02$ , with the exact value depending on the dispersed phase solutions. The transitional  $Ca_c$  values from the dripping to jetting regimes were found to have a larger variation with the dispersed phase solutions used. Generally, a dispersed phase with a higher viscosity (larger viscosity ratio) is accompanied by a smaller transitional  $Ca_c$  from the dripping to jetting regimes, which is in agreement with the experimental results of Bashir *et al.*[2]. This is likely due to the higher dispersed phase viscosity enhancing the stability of the interface leading to a higher  $Ca_c$  to induce jetting. This method was applied to published data [8] and the results are given in figure 5, which confirmed that the transitional  $Ca_c$  from the dripping to jetting regimes is reduced as the viscosity ratio increases.

#### Drop Velocity after Drop Formation

The position of the drop in the continuous phase channel was tracked and the velocity 1.5 mm downstream of the T-junction is plotted in figure 6. As the dimensionless drop diameter increases, the relative velocity of the drop decreases. It is expected that as the drop diameter increases, more of the channel will be occupied by the drop, hence the continuous phase should

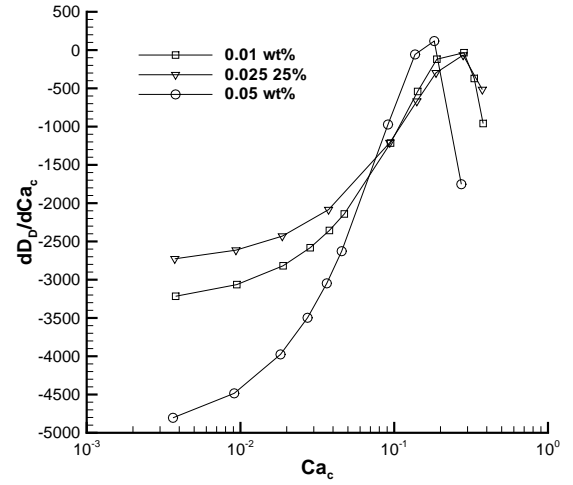


Figure 3: The gradient of the drop diameter with varying  $Ca_c$  and wt % XG concentrations. The lines are there to act as a guide.

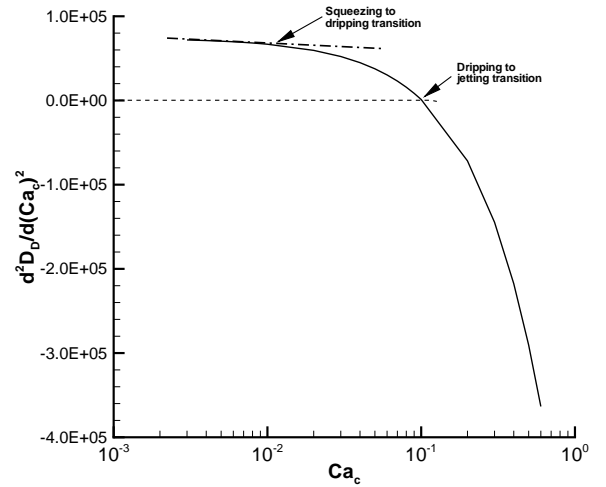


Figure 4:  $d^2D_D/dCa_c^2$  with varying  $Ca_c$  for a 0.05 wt % XG. The upper dotted line intersection with the curve provides an estimate of the squeezing to dripping transition  $Ca_c$  and  $d^2D_D/dCa_c^2 = 0$  provides the transition  $Ca_c$  for dripping to jetting.

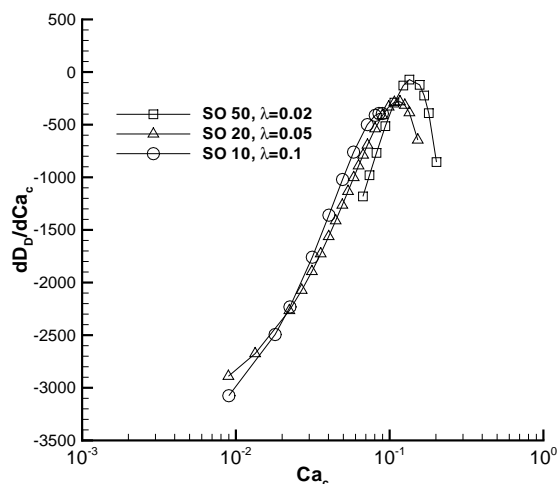


Figure 5: Slopes of the data from Husny and Cooper-White [8]. Water was the dispersed phase with silicone oils (SO) of different viscosities as the continuous phase. The location of the  $Ca_c$  for which  $dDD/dCa_c$  is a maximum, indicating dripping to jetting transition, increases with decreasing  $\lambda$ . The lines are there to as a guide.

act as a piston of fluid to move the drop downstream. If the drop fully occupies the channel, then the drop would then be travelling at the average velocity of the fluid in the continuous phase channel. For the continuous phase channel, the maximum velocity at the centre of the channel is 1.98 times the average velocity which is close to the velocities attained by drops with a dimensionless drop diameter less than about 0.25.

### Conclusions

The use of XG for the disperse phase fluid has shown that an increase in the disperse phase fluid viscosity does not have a strong effect on the drop size compared to water. The drop size is usually smaller than when water is used and the difference increases with increasing  $Ca_c$ . A method was proposed for delineating the different drop formation regimes by differentiating the drop size with  $Ca_c$  and it was found to be applicable to other published results.

### Acknowledgments

Z. Gu gratefully acknowledges the financial support from the Research Publication Fellowships (UNSW) and Chinese Scholarship Council.

### References

- [1] Anna, S. L., Bontoux, N. and Stone, H. A., Formation of dispersions using “flow focusing” in microchannels, *Appl Phys Lett*, **82**, 2003, 364–366.
- [2] Bashir, S., Rees, J. M. and Zimmerman, W. B., Simulations of microfluidic droplet formation using the two-phase level set method, *Chem Eng Sci*, **66**, 2011, 4733–4741.
- [3] Christopher, G. F. and Anna S. L., Microfluidic methods for generating continuous droplet stream, *Journal of Physics D-Applied Physics*, **40**, 2007, R319–R336.

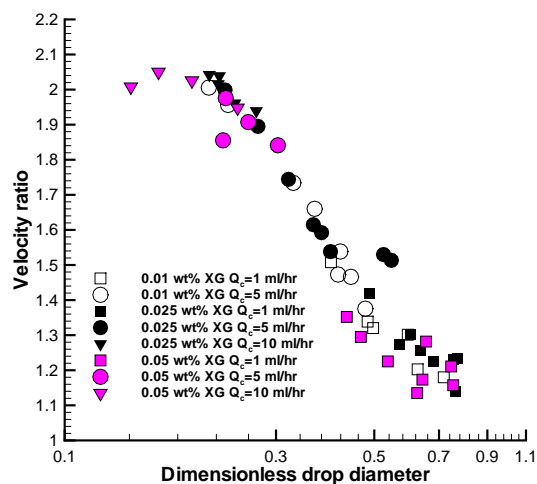


Figure 6: Velocity of the drop 1.5 mm downstream of the T-junction as a ratio of the average velocity of the fluid in the outlet channel.

- [4] De Menech, M., Garstecki, P., Jousse, F. and Stone, H. A., Transition from squeezing to dripping in a microfluidic T-shaped junction, *Journal of Fluid Mechanics*, **595**, 2008, 141–161.
- [5] Garstecki, P., Fuerstman, M. J., Stone, H. A. and Whitesides, G. M., Formation of droplets and bubbles in a microfluidic T-junction – scaling and mechanism of breakup, *Lab on a Chip*, **6**, 2006, 437–446.
- [6] Glawdel, T., Elbuken, C. and Ren, C. L., Droplet formation in microfluidic T-junction generators operating in the transitional regime. I. Experimental observations, *Phys. Rev. E*, **85**, 2012, 016322.
- [7] Hong, J. S. and Cooper-White, J., Drop formation of Carbopol dispersions displaying yield stress, shear thinning and elastic properties in a flow-focusing microfluidic channel, *Korea-Australia Rheology Journal*, **21**, 2009, 269–280.
- [8] Husny, J. and Cooper-White, J. J., The effect of elasticity on drop creation in T-shaped microchannels, *Journal of Non-Newtonian Fluid Mechanics*, **137**, 2006, 121–136.
- [9] Liow, J. L., Mechanical micromachining: a sustainable micro-device manufacturing approach? *Journal of Cleaner Production*, **17**, 2009, 662–667.
- [10] Raj, R., Mathur, N. and Buwa, V.V., Numerical simulations of liquid-liquid flows in microchannels. *Ind. Eng. Chem. Res.*, **49**, 2010, 10606–10614.
- [11] Xu, J. H., Li, S. W., Tan, J., Wang, Y. J. and Luo, G. S., Preparation of highly monodisperse droplet in a T-junction microfluidic device, *AIChE Journal*, **52**, 2006, 3005–3010.
- [12] Yeom, S. and Lee, S. Y., Size prediction of drops formed by dripping at a micro T-junction in liquid-liquid mixing, *Exp. Therm. Fluid Sci.*, **35**, 2011, 387–394.